Solar RRL
www.solar-rrl.com

Direct Observation of the Chemical Transformations in $BiVO_4$ Photoanodes upon Prolonged Light-Aging Treatments

Ramón Arcas, Drialys Cardenas-Morcoso, Maria Chiara Spadaro, Miguel García-Tecedor, Camilo A. Mesa, Jordi Arbiol, Francisco Fabregat-Santiago, Sixto Giménez,* and Elena Mas-Marzá**

Exposing $BiVO_4$ photoanodes to light-aging treatments is known to produce a significant photocurrent enhancement. Until now, the interpretation given to this phenomenon is associated to the formation of oxygen vacancies and little is reported about chemical changes in the material. Herein, the chemical segregation of Bi species toward the surface upon light-aging treatment is demonstrated, which takes place with the concomitant formation of intra-bandgap states associated to the oxygen vacancies. It is further demonstrated that these intra-bandgap states are photoactive and generate photocurrent under infrared excitation. These results highlight the importance of understanding light-induced effects while employing multinary metal oxide photoelectrodes.

1. Introduction

Photoelectrocatalysis (PEC) has emerged as an attractive route to store solar energy involving photoelectro-oxidation and photoelectro-reduction processes. To date, most of the PEC applications developed have been mainly focused either on water splitting to obtain molecular hydrogen[1] or on the reduction of CO_2 to C1 and C2 derivatives.[2] However, there is a growing interest to exploit alternative reactions to obtain compounds with higher added value for the chemical industry.[3,4] Among the different transformations proposed, the PEC oxidation of primary alcohols to the corresponding aldehydes or acids has attracted significant attention.[5–8] $BiVO_4$ is a promising material for the development of PEC devices, mainly due to its suitable bandgap (2.4 eV), which allows visible light absorption (up to 516 nm)[9] leading to a theoretical photocurrent of $\approx 7.5\ mA\ cm^{-2}$ under 1 sun illumination.[10] Furthermore, its band structure (i.e., the position of the valence and conduction bands) leads to large photovoltages for driving organic transformations.[11–13] In contrast, the low electron mobility has been identified as the main bottleneck for the PEC performance of this material.[14,15]

The crystal structure of $BiVO_4$ is composed by Bi^{3+} and V^{5+} cations in coordination with O^{2-}.[16] During structural arrangement, the inherent formation of structural defects takes place and their concentration can be controlled by either modifying the synthetic conditions[17] or by post-synthetic treatments.[18,19] The most common defects in this material are oxygen vacancies (OV_s), which are the result of removing O atoms from the lattice.[20–22] It has been shown that these OV_s have a huge impact on the PEC behavior of different photoanodes for the oxygen evolution reaction (OER).[23–26] Specifically, the effect of OV_s on $BiVO_4$ for OER is based on the ability of these defects to increase the bulk carrier concentration and conductivity.[27] Furthermore, an excessive density of OV_s has been correlated to the decrease of performance.[28] The formation of OV_s also creates intra-bandgap states, mainly related to V species, where the electrons are located closer to the conduction band.[29] These new electronic states lead to enhanced light absorption and have been related to the reduction of the nearby vanadium atoms from V_{ov}^{5+} to V_{ov}^{4+}.[30] The attempts to directly excite these

R. Arcas, C. A. Mesa, F. Fabregat-Santiago, S. Giménez, E. Mas-Marzá
Institute of Advanced Materials (INAM)
Universitat Jaume I
12006 Castelló, Spain
E-mail: cmesa@uji.es; sjulia@uji.es; emas@uji.es

D. Cardenas-Morcoso
Material Research and Technology (MRT) Department
Luxembourg Institute of Science and Technology (LIST)
4422 Belvaux, Luxembourg

M. C. Spadaro, J. Arbiol
Catalan Institute of Nanoscience and Nanotechnology (ICN2)
CSIC and BIST
08193 Barcelona, Catalonia, Spain

M. García-Tecedor
Unidad de Procesos Fotoactivados
Instituto IMDEA Energía
28935 Móstoles, Madrid, Spain

J. Arbiol
Advanced Electron Nanoscopy (GAeN)
ICREA
08010 Barcelona, Catalonia, Spain

The ORCID identification number(s) for the author(s) of this article can be found under https://doi.org/10.1002/solr.202200132.

DOI: 10.1002/solr.202200132

intra-bandgap states associated with oxygen vacancies in $BiVO_4$ have been limited, and only a recent study by Selim et al. reports the use of a transient infrared light to modulate the electrical response of the photoanode.[30] Consequently, infrared excitation of OV_s could clarify the role of these chemical defects on the PEC performance of $BiVO_4$.

In contrast, prolonged light-aging (LA) treatments have been reported to improve the PEC performance of $BiVO_4$ toward OER. Trzésniewski et al. showed the enhancement of both photocurrent and photovoltage for undoped and uncatalyzed $BiVO_4$ photoanodes due to a process the authors refer as photocharging (10 h under illumination at open-circuit conditions).[31] Similar results were reported by Li et al. after 20 h of curing under ultraviolet (UV) illumination.[32] In both studies, the authors attributed the increase in photocurrent to the reduction of surface recombination processes as a consequence of the decrease of the defect sites at the surface.[33] The effects of the LA treatments were also analyzed by Liu et al. using Intensity-Modulated Photocurrent Spectroscopy (IMPS).[34] The authors found that after 3 h of light treatment, a complex interaction between charge transfer and surface recombination takes place, dominating the suppression of surface recombination at more positive applied potentials. More recently, Feng et al. reported the beneficial effects of a photoetching treatment, consisting of 10 min illumination at open-circuit conditions. This treatment revealed that short illumination periods generates OV_s at the surface, which double the $BiVO_4$ photocurrent due to the significant enhancement of the charge separation efficiency.[35] All these studies demonstrated that short periods (10 min to 20 h) of LA preferentially modify the $BiVO_4$ surface; however, illumination periods longer than 30 h have not been reported yet.

Few works have tried to analyze the influence of LA treatments on $BiVO_4$ using in situ spectroelectrochemical measurements. Particularly, Firet et al. employing a sequence of X-ray photoelectron spectroscopy (XPS), UV–vis, and X-ray raman scattering (XRS) techniques[36] and Venugopal et al. using infrared spectroscopy[37] revealed a dynamic nature of the light treatments on $BiVO_4$/electrolyte interface; however, in these cases, the effect of the electrolyte could mask the true effects of light into the material during the LA process.

In the present study, we report the effect of prolonged light treatments on the PEC behavior of $BiVO_4$ photoelectrodes for the benzyl alcohol oxidation under air conditions for 48 h. We have selected this reaction as a model platform for more complex organic transformations, opening the door to more sustainable and environmentally friendly synthetic strategies. Morphological, structural, and electrical measurements allowed us to unravel the different chemical processes taking place in the material during the light treatment and correlate them with the changes observed in PEC response. Moreover, we show for the first time, to the best of our knowledge, steady-state photocurrent generation upon continuous infrared (IR) excitation, confirming the photoactivity of these light-induced electronic states.

2. Results and Discussion

$BiVO_4$ photoanodes were prepared by electrodeposition on fluorine doped tin oxide (FTO) substrates, as detailed in the Supporting Information (S.I.), and were illuminated in air to elucidate the influence of prolonged LA treatments for the oxidation of benzyl alcohol. Our $BiVO_4$ photoanodes were illuminated at two different light intensities (1 and 3 suns for 1LA–$BiVO_4$ and 3LA–$BiVO_4$, respectively) for 48 h, while the other films were kept under dark conditions (Reference). All samples were tested using the operational conditions normally used to oxidize selectively benzyl alcohol to benzaldehyde.[6] A 0.1 M tetrabutylammonium perchlorate ($TBAClO_4$) in CH_3CN solution served as nonaqueous electrolyte to avoid the competing water oxidation reaction. A UV filter was incorporated to the ozone-free Xe lamp to avoid the singlet oxygen generation and the non-faradaic oxidation of benzyl alcohol, previously reported for a similar system.[5] **Figure 1** compares the photocurrent of 1LA–$BiVO_4$ and 3LA–$BiVO_4$ to that for the Reference, showing a performance enhancement after the LA treatment. Similarly, the LA treatment produced films with higher photocurrents toward the OER as shown in Figure S2, Supporting Information. The difference in the onset potential between LA and Reference sample observed for OER and not present in alcohol (ROH) oxidation demonstrates the higher catalytic activity of $BiVO_4$ photoanodes toward alcohol oxidation compared to OER.

To study the nature of the LA treatment on $BiVO_4$, we first analyzed the morphology and crystalline structure of $BiVO_4$ by scanning electron microscopy (SEM), see **Figure 2**a,b and S3, Supporting Information. A clear change in the surface of the $BiVO_4$ photoanodes is observed after LA. More precisely, while the Reference $BiVO_4$ exhibits a homogenous surface (Figure 2a), the LA samples are characterized by the presence of several islands (region B in Figure 2b) formed by small nanoparticles surrounding the regular $BiVO_4$ grains. Interestingly, energy dispersive X-ray spectroscopy (EDS) analysis for the different samples (Figure 2c) revealed that upon LA treatment, the stoichiometric Bi/V concentration ratio of the Reference $BiVO_4$ divides into Bi-deficient (zone A in Figure 2b) and

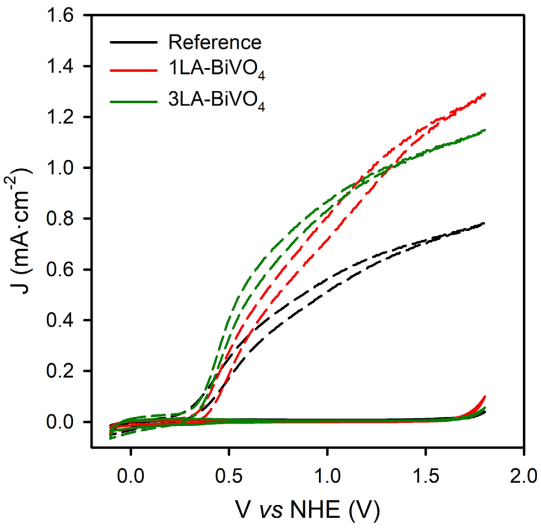

Figure 1. Cyclic voltammograms of Reference (black), 1LA–$BiVO_4$ (red) and 3LA–$BiVO_4$ (green) photoanodes measured at 20 mV s^{-1} in 0.1 M benzyl alcohol in acetonitrile solution with 0.1 M tetrabutylammonium perchlorate ($TBAClO_4$) in the dark (solid lines) and under illumination (100 mW cm^{-2}) [dashed lines].

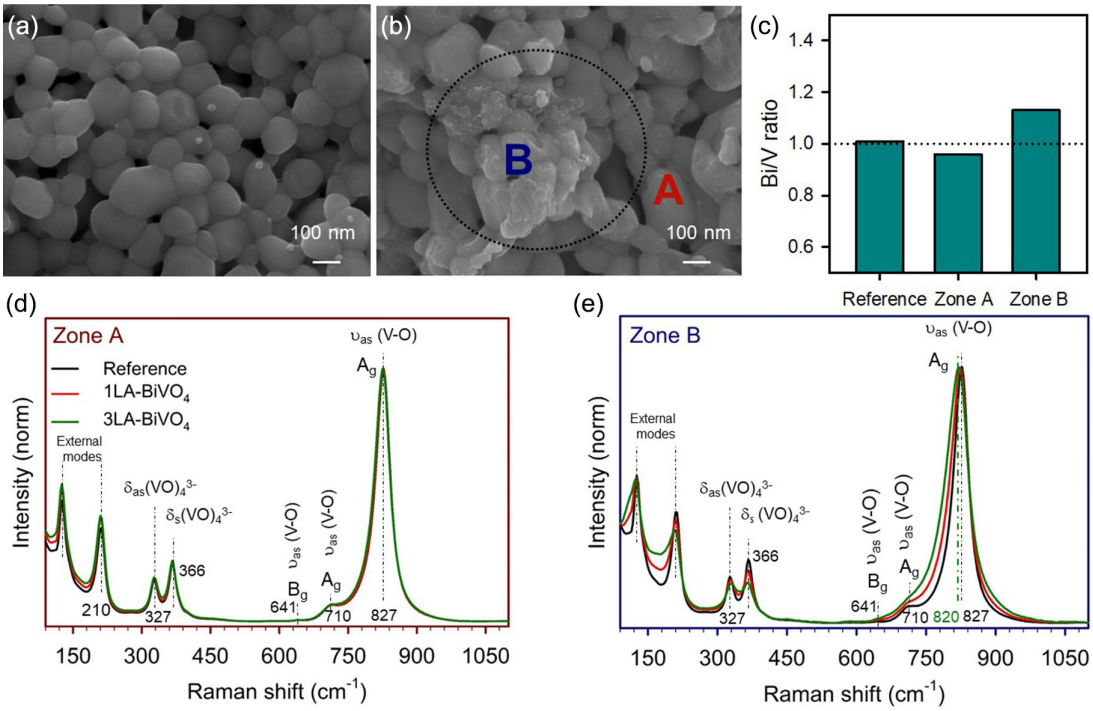

Figure 2. Top-view scanning electron microscope (SEM) images of a) Reference and b) 1LA–$BiVO_4$. c) Bi/V concentration ratio for Reference and A and B zones measured by EDS in (b). Raman spectra of d) Zone A and e) Zone B.

Bi-enriched domains (zone B in Figure 2b). These observations evidence the morphological and chemical modification of the $BiVO_4$ photoanodes due to LA and are directly related to the photocurrent increase shown in Figure 1.

To further analyze the morphological and chemical modifications of $BiVO_4$ photoanodes induced by LA treatment, we performed Raman spectroscopy on all samples in both zones A and B in Figure 2b. As depicted in Figure 2d,e, Raman bands perfectly matched with the vibrational modes of $BiVO_4$.[38,39] Comparing the different samples, Raman bands were practically independent of LA in zone A. However, a significant band broadening is observed in zone B after LA, in particular, for both the external and A_g modes. This has been previously attributed to the formation of defects, such as oxygen vacancies or hydrogen impurities.[40,41] We note that oxygen vacancies in metal oxides can also be monitored by other techniques like electron paramagnetic resonance (EPR), [42,43] cathodoluminescence,[44] transient absorption spectroscopy (TAS),[28] and spectroelectrochemistry.[45] In contrast, X-ray diffraction (XRD) measurements did not evidence any relevant modification of the crystalline structure due to LA (Figure S4, Supporting Information).

We move now to investigate the morphological transformation upon LA by transmission electron microscopy (TEM). Indeed, compared to the homogeneous surface of the Reference $BiVO_4$ sample (**Figure 3**a), 1LA-$BiVO_4$ evidenced the development of a thin amorphous layer, as the origin of the growth of small nanoparticles, as observed in Figure 3b, on the $BiVO_4$ crystallites, which results in a granulated surface (Figure 3c). Additionally, scanning TEM (STEM) combined with electron energy loss spectroscopy (STEM–EELS) proved the increase of Bi species on the surface of $BiVO_4$ crystallites after LA (Figure S5, Supporting Information). It is apparent from Figure 3 that prolonged electron-beam irradiation undergoes in a dramatic morphological transformation of our $BiVO_4$. Interestingly, migration of some atomic species from the bulk to form particles at the surface could be recorded during the electron beam irradiation (the complete sequence can be visualized in the video freely available at 10.5281/zenodo.5643642) and the final morphology presented the segregation of a significant number of nanoparticles on top of the $BiVO_4$ grains (Figure 3c,d).

To understand the nature and composition of these aggregates, we carried out a detailed high-resolution TEM (HR-TEM) characterization. Figure 3e shows the HR-TEM image of the bulk area of a $BiVO_4$ grain. The power spectrum (fast Fourier transform) analysis of this area (inset in Figure 3e) confirms the monoclinic clinobisvanite $BiVO_4$ phase I112/B (s.g. 15) oriented along its [011] zone axis. However, focusing the electron beam on the segregated nanoparticles (Figure 3f), the power spectrum analysis clearly indicates the presence of Bi species. The results of the power spectra analysis in different areas matched with two different Bi structures: metallic Bi with hexagonal structure (R3-MH s.g. 166) oriented along [241] and [5–51] and monoclinic Bi_2O_3 oriented along [110] and [–114] zone axis, indicating the plausible chemical composition of this segregated particles (see Figure S6, Supporting Information).

We note that the electron beam in both SEM and TEM measurements is clearly different in wavelengths and intensities compared to sunlight (LA treatment). However, the morphology and presence of Bi-rich particles at the surface on the LA-treated

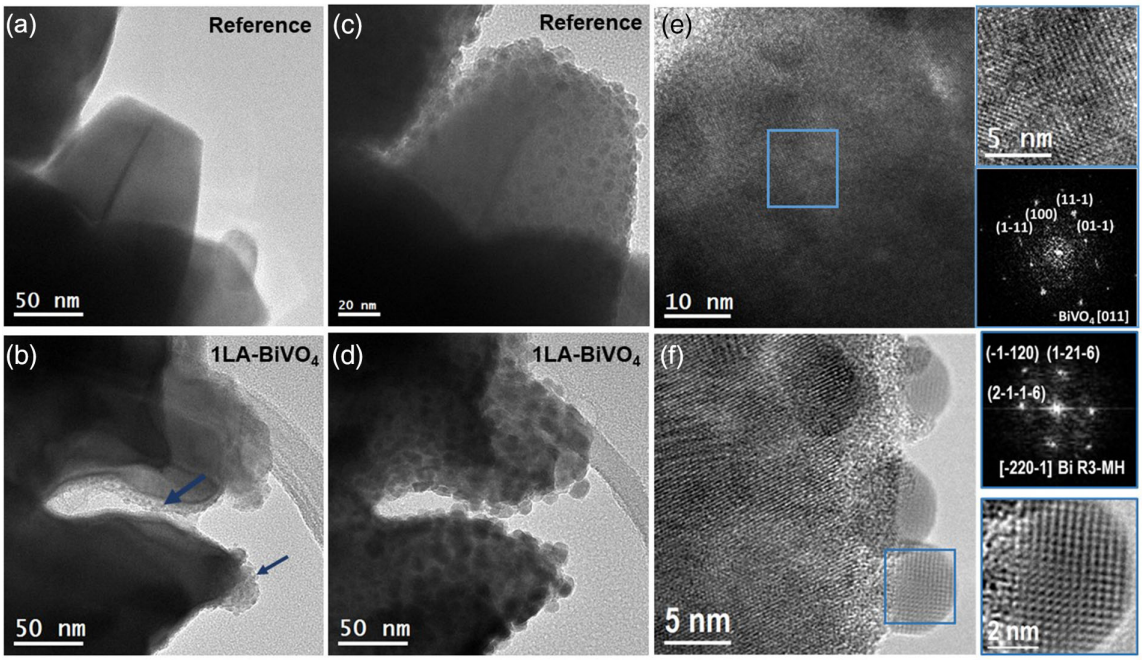

Figure 3. Transmission electron microscope (TEM) images a,b) before and c,d) after electron-beam irradiation. a,c) correspond to the Reference and b,d) correspond to the 1LA–$BiVO_4$, demonstrating that the $BiVO_4$ morphology transforms during either light or electron-beam irradiation. e,f) High-resolution TEM (HR-TEM) and power spectra images of bulk and surface $BiVO_4$ grains, respectively, after electron-beam irradiation.

sample (Figure S5, Supporting Information) suggest that the localized structural modification induced by LA is alike to that presented after electron-beam irradiation, involving in both cases the segregation of Bi species.

Summarizing, we have shown by different spectroscopic and microscopic techniques that LA induces OV_S and a Bi segregation process. These processes have been reported previously in different studies, where $BiVO_4$ has undergone prolonged exposure to light, including light treatment studies at open-circuit conditions and stability tests under operational conditions.[18,25,31,33,35,36,46] In all cases, different morphological and compositional processes take place at the electrode in different electrolytes and in different structures of $BiVO_4$ converging in a higher proportion of Bi compared to V.

Now, we turn to investigate plausible mechanistic insights of the effect of LA on the functional performance of the photoanodes (as showed in Figure 1). To this end, we perform Impedance Spectroscopy (IS) measurements under illumination to extract Nyquist plots, at different potentials, relevant for the selective oxidation of benzyl alcohol to benzaldehyde. **Figure 4**a shows one of the experimentally obtained Nyquist plot and the selected equivalent circuit (inset) used to fit the data, which has been generally employed for different metal oxide photoanodes.[47] This equivalent circuit is commonly used to separate the contribution of bulk and surface processes in the photoanodes.[33] The elements employed are R_s (series resistance), C_{bulk} (bulk capacitance), R_{bulk} (bulk resistance), R_{ct} (charge transfer resistance), and C_s (surface capacitance). The obtained capacitances and resistances as a function of the applied potential are reported in Figure S7 and S8, Supporting Information.

Figure 4b and S7a, Supporting Information, show the presence of two peaks at 0.35 and 0.75 V versus normal hydrogen electrode (NHE), for the surface capacitance (C_s light green empty circles in Figure 4b) of all tested samples. The peak at 0.35 V is coincident with the valley of the R_{ct} (dark green empty circles in Figure 4b), and both features take place at the same potential associated to the benzyl alcohol oxidation onset (dark green full cycles). A similar behavior has been already observed in different metal oxides, where a surface capacitance peak is observed just before the onset for OER. This behavior on hematite photoanodes was assigned to charge transfer controlled by surface state charging associated to intermediate species in the reaction process.[47] Consequently, we suggest that alcohol oxidation is controlled by a surface state, which dictates the hole transfer process from the electrode to the substrate. We note that the height of this peak, associated to the Density Of electronic States (DOS) at the surface, is lower for the 1LA–$BiVO_4$ sample compared to the Reference sample. A more detailed study of the influence of this surface capacitance on the photoelectrooxidation of benzyl alcohol remains beyond the scope of the present work.

In contrast, the broader peak at 0.75 V versus NHE either in C_s and C_{bulk} is assigned to the V^{4+}/V^{5+} redox process, which has previously been related to the presence of OV_s in $BiVO_4$ films.[33,48,49] The presence of this peak in the reference sample suggests the intrinsic formation of these defects during the crystallization step.

Considering C_s, the DOS of these surface vancancies, $g(E_{Fn})$, can be estimated by Equation (1)

$$C_s = qg(E_{Fn}) \quad (1)$$

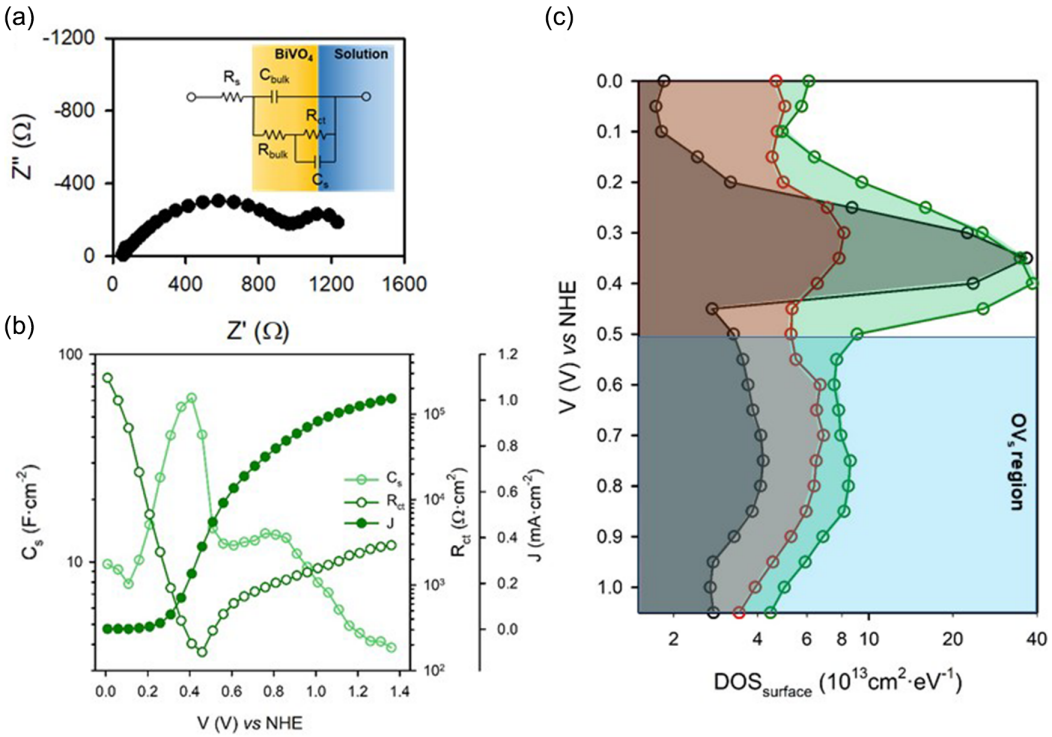

Figure 4. a) Nyquist plot of Reference sample and selected equivalent circuit to fit the experimental data of the Reference and LA samples. b) Surface capacitance (C_s), charge transfer resistance (R_{ct}), and photocurrent (J) of Reference $BiVO_4$. c) Density of surface states as a function of applied potential. Reference (Black), 1LA–$BiVO_4$ (Red) and 3LA–$BiVO_4$ (Green). Measurements were performed under illumination, in 0.1 M benzyl alcohol oxidation conditions.

where q is the elementary charge (1.6×10^{-19} C). Figure 4c shows that the calculated DOS associated to OV_s scales with the irradiation intensity, confirming the increase of the V^{4+} species during the LA process as mentioned previously in Raman. This result, in agreement with our Raman measurements, confirms the modification of the electronic environment of $BiVO_4$ during the LA. These observations are consistent with the results reported by Feng et al.[35] although, the higher concentration of OV_s, reflected on the bulk capacitance suggests that prolonged LA affects not only the bulk but also the surface of the film. Such higher OV_s concentration could also be responsible for the slightly lower photocurrent density found for the 3LA–$BiVO_4$ sample in Figure 1. This is supported by the detrimental role of a "too high" concentration of OV_s in $BiVO_4$ photoanodes, as previously suggested,[23,41] being also consistent with a recent report by Corby et al. in which an excessive concentration of OV_s could be negative for the PEC performance of WO_3 photoanodes,[28] suggesting that this effect may be general for metal oxide photoelectrodes. Furthermore, we have performed a long LA treatment (LT) for 3 weeks under 1 sun illumination (LT–1LA–$BiVO_4$, Figure S9, Supporting Information), which compared to 1LA–$BiVO_4$ leads to an increased DOS of OV_s, and lower photocurrent, also in good agreement with this hypothesis. Collectively, our observations also suggest the possibility that above certain levels, Bi segregation at the surface of the $BiVO_4$ could impede the charge transfer of holes to the solution. In this case, the Bi species on the surface of $BiVO_4$ could operate as a blocking layer for surface states as shown in Figure S7, Supporting Information.

Finally, to confirm the generation of new intra-bandgap electronic states associated with OV_s in $BiVO_4$, we used an IR continuous-wave laser as light source to extract steady-state photocurrents for the oxidation of benzyl alcohol. Upon sub-bandgap excitation, photocurrent generation can only be due to the activation of intra-bandgap transitions in the semiconductor material (see Figure S10, Supporting Information). This approach, to the best of our knowledge, uses for the first-time IR radiation (980 nm, 1.26 eV) to selectively excite the trapped electrons from the intra-bandgap states to the conduction band. **Figure 5**a shows the IR-chopped chronoamperometry measurements for Reference and 3LA–$BiVO_4$ samples at 0.8 V versus NHE. The measured photocurrent stems from the excitation of the intra-bandgap states. The highest photocurrent of the 3LA–$BiVO_4$ sample is fully consistent with its increased density of intra-bandgap states, associated with OV_s (Figure 5b). Surprisingly, the photocurrent of the 3LA–$BiVO_4$ sample almost doubled compared to that for the Reference (from ≈50 to ≈90 nA cm^{-2}). This is in excellent agreement with the equivalent increase of the DOS (from ≈4 to ≈8×10^{13} cm^2 eV^{-1}) associated to OV_s (Figure 4c).

We note that, although surface reduction of $BiVO_4$[50] and the increase of surface Bi species[25,51] have been previously reported, both effects have been characterized either after or during operando conditions and, consequently, they were attributed to vanadium dissolution.[37] On the contrary, the LA treatments and the structural characterization performed here take place in the absence of electrolyte. Therefore, the bismuth-rich surface observed is a direct consequence of the incidence of light on

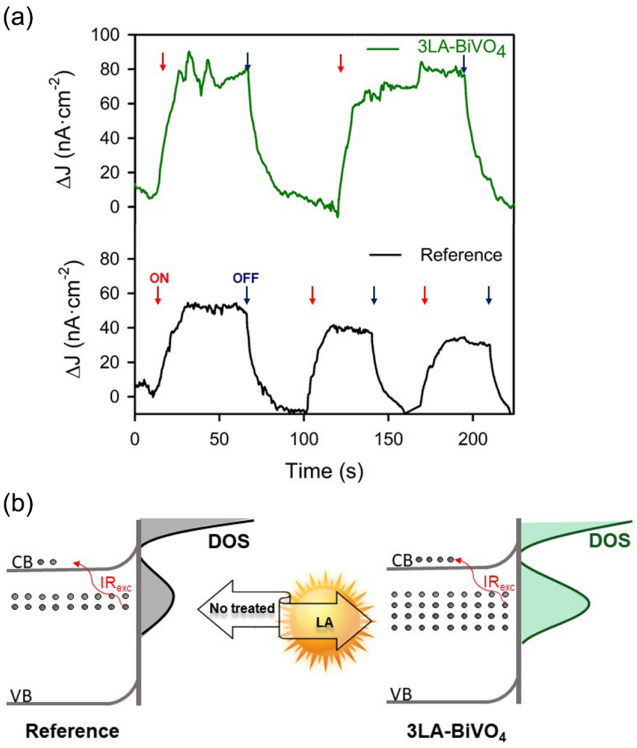

Figure 5. a) Infrared (IR)-chopped chronoamperometry measurements of Reference (Black) and 3LA-$BiVO_4$ (green). b) Band diagrams representation of the fresh and light-aged-treated $BiVO_4$ samples.

$BiVO_4$. Moreover, we demonstrate the correlation between the segregation of small Bi-rich nanoparticles and the formation of new intra-bandgap states associated to oxygen vacancies. The photoactivity of these intra-bandgap states observed under IR illumination opens new perspectives for the development of competitive $BiVO_4$ photoanodes.

3. Conclusion

Herein, we have investigated the effeect of prolonged light-aging (LA) on $BiVO_4$ photoanodes, providing a direct observation of the chemical and structural modifications after LA treatments. We showed that light-assisted treatments under air conditions led to the chemical transformation of the material, which depended on the light intensity used during the LA. Electrical, PEC and HR-TEM characterizations allowed assigning the chemical transformations observed to the segregation of Bi species on top of $BiVO_4$ grains, leading to the formation of new intra-bandgap states associated to oxygen vacancies. Moreover, effective photocurrent generation from these intra-bandgap states was demonstrated by IR light excitation, confirming the formation of oxygen vacancies during the LA treatment and their implications on the generation of IR photocurrent. These results highlight the importance of understanding the light-induced effects while employing multinary metal oxide photoelectrodes either for OER or for the synthesis of high added-value chemicals.

Supporting Information

Supporting Information is available from the Wiley Online Library or from the author.

Acknowledgements

The authors thank support from the projects ENE2017-85087-C3-1-R, PID2020-116093RB-C41, PID2020-116093RB -C43 and Network of Excellence CAT&SCALE (RED2018-102459-T), funded by MCIN/ AEI/ 10.13039/501100011033. University Jaume I (UJI-B2019-20) and Generalitat Valenciana (PROMETEO/2020/028) are also acknowledged for financial support. Serveis Centrals d'Instrumentació Científica from UJI are also acknowledged for SEM, TEM, Raman, and XRD measurements. M.C.S. and J.A. acknowledge funding from Generalitat de Catalunya 2017 SGR 327. ICN2 is supported by the Severo Ochoa program from Spanish MINECO (Grant no. SEV-2017-0706) and is funded by the CERCA Programme/Generalitat de Catalunya. M.C.S. has received funding from the European Union's Horizon 2020 research and innovation programme under the Marie Skłodowska-Curie Grant Agreement no. 754510 (PROBIST) and the Severo Ochoa programme. C.A.M. acknowledges the University Jaume I for the postdoc fellowship POSDOC/ 2019/20 and Generalitat Valenciana for the APOSTD/2021/251 fellowship. Dr. Beatriz Julián-López and Laura Montañés are also acknowledged for their help with the measurements with the infrared laser beam and some electrodes preparation.

Conflict of Interest

The authors declare no conflict of interest.

Data Availability Statement

The data that support the findings of this study are available from the corresponding author upon reasonable request.

Keywords

Bi segregation, $BiVO_4$, light-aging treatments, oxygen vacancies

Received: February 11, 2022
Revised: March 7, 2022
Published online: March 20, 2022

[1] M. Grätzel, *Nature* **2001**, *414*, 338.
[2] B. Kumar, M. Llorente, J. Froehlich, T. Dang, A. Sathrum, C. P. Kubiak, *Annu. Rev. Phys. Chem.* **2012**, *63*, 541.
[3] K. Sayama, *ACS Energy Lett.* **2018**, *3*, 1093.
[4] C. R. Lhermitte, K. Sivula, *ACS Catal.* **2019**, *9*, 2007.
[5] R. Arcas, E. Peris, E. Mas-Marzá, F. Fabregat-Santiago, *Sustain. Energy Fuels* **2021**, *5*, 956.
[6] T. Li, T. Kasahara, J. He, K. E. Dettelbach, G. M. Sammis, C. P. Berlinguette, *Nat. Commun.* **2017**, *8*, 1.
[7] H. G. Cha, K. S. Choi, *Nat. Chem.* **2015**, *7*, 328.
[8] D. Liu, J. C. Liu, W. Cai, J. Ma, H. Bin Yang, H. Xiao, J. Li, Y. Xiong, Y. Huang, B. Liu, *Nat. Commun.* **2019**, *10*, 1779.
[9] M. Long, W. Cai, H. Kisch, *J. Phys. Chem. C* **2008**, *112*, 548.
[10] J. H. Kim, J. S. Lee, *Adv. Mater.* **2019**, *31*, 1806938.
[11] J. K. Cooper, S. Gul, F. M. Toma, L. Chen, Y. S. Liu, J. Guo, J. W. Ager, J. Yano, I. D. Sharp, *J. Phys. Chem. C* **2015**, *119*, 2969.

[12] J. K. Cooper, S. Gul, F. M. Toma, L. Chen, P. A. Glans, J. Guo, J. W. Ager, J. Yano, I. D. Sharp, *Chem. Mater.* **2014**, *26*, 5365.
[13] Z. Zhao, Z. Li, Z. Zou, *Phys. Chem. Chem. Phys.* **2011**, *13*, 4746.
[14] F. F. Abdi, T. J. Savenije, M. M. May, B. Dam, R. Van De Krol, *J. Phys. Chem. Lett.* **2013**, *4*, 2752.
[15] M. Ziwritsch, S. Müller, H. Hempel, T. Unold, F. F. Abdi, R. van de Krol, D. Friedrich, R. Eichberger, *ACS Energy Lett.* **2016**, *1*, 888.
[16] W. Luo, J. Wang, X. Zhao, Z. Zhao, Z. Li, Z. Zou, *Phys. Chem. Chem. Phys.* **2013**, *15*, 1006.
[17] J. M. Wu, Y. Chen, L. Pan, P. Wang, Y. Cui, D. C. Kong, L. Wang, X. Zhang, J. J. Zou, *Appl. Catal., B Environ.* **2018**, *221*, 187.
[18] M. Lamers, S. Fiechter, D. Friedrich, F. F. Abdi, R. Van De Krol, *J. Mater. Chem. A* **2018**, *6*, 18694.
[19] B. Lamm, B. J. Trześniewski, H. Döscher, W. A. Smith, M. Stefik, *ACS Energy Lett.* **2017**, *3*, 112.
[20] Z. Wang, X. Mao, P. Chen, M. Xiao, S. A. Monny, S. Wang, M. Konarova, A. Du, L. Wang, *Angew. Chem., Int. Ed.* **2019**, *58*, 1030.
[21] J. Gan, X. Lu, J. Wu, S. Xie, T. Zhai, M. Yu, Z. Zhang, Y. Mao, S. C. I. Wang, Y. Shen, Y. Tong, *Sci. Rep.* **2013**, *3*, 1021.
[22] M. L. Crespillo, J. T. Graham, F. Agulló-López, Y. Zhang, W. J. Weber, *Appl. Mater. Today* **2018**, *12*, 131.
[23] R. Fernández-Climent, S. Giménez, M. García-Tecedor, *Sustain. Energy Fuels* **2020**, *4*, 5916.
[24] W. Wang, P. J. Strohbeen, D. Lee, C. Zhou, J. K. Kawasaki, K.-S. Choi, M. Liu, G. Galli, *Chem. Mater.* **2020**, *32*, 2899.
[25] R. Gao, L. Wang, *Angew. Chem. Int. Ed.* **2020**, *59*, 23094.
[26] C. A. Mesa, L. Steier, B. Moss, L. Francàs, J. E. Thorne, M. Grätzel, J. R. Durrant, *J. Phys. Chem. Lett.* **2020**, *11*, 7285.
[27] H. Seo, Y. Ping, G. Galli, *Chem. Mater.* **2018**, *30*, 7793.
[28] S. Corby, L. Francàs, A. Kafizas, J. R. Durrant, *Chem. Sci.* **2020**, *11*, 2907.
[29] A. Walsh, Y. Yan, M. N. Huda, M. M. Al-Jassim, S.-H. Wei, *Chem. Mater.* **2009**, *21*, 547.
[30] S. Selim, E. Pastor, M. García-Tecedor, M. R. Morris, L. Francàs, M. Sachs, B. Moss, S. Corby, C. A. Mesa, S. Gimenez, A. Kafizas, A. A. Bakulin, J. R. Durrant, *J. Am. Chem. Soc.* **2019**, *141*, 18791.
[31] B. J. Trześniewski, W. A. Smith, *J. Mater. Chem. A* **2016**, *4*, 2919.
[32] T. Li, J. He, B. Peña, C. P. Berlinguette, *Angew. Chem., Int. Ed.* **2016**, *55*, 1769.
[33] B. J. Trześniewski, I. A. Digdaya, T. Nagaki, S. Ravishankar, I. Herraiz-Cardona, D. A. Vermaas, A. Longo, S. Gimenez, W. A. Smith, *Energy Environ. Sci.* **2017**, *10*, 1517.
[34] E. Y. Liu, J. E. Thorne, Y. He, D. Wang, *ACS Appl. Mater. Interfaces* **2017**, *9*, 22083.
[35] S. Feng, T. Wang, B. Liu, C. Hu, L. Li, Z. Zhao, J. Gong, *Angew. Chem., Int. Ed.* **2020**, *59*, 2044.
[36] N. J. Firet, A. Venugopal, M. A. Blommaert, C. Cavallari, C. J. Sahle, A. Longo, W. A. Smith, *Chem. Mater.* **2019**, *31*, 7453.
[37] A. Venugopal, R. Kas, K. Hau, W. A. Smith, *J. Am. Chem. Soc.* **2021**, *143*, 18581.
[38] D. Zhou, L. X. Pang, W. G. Qu, C. A. Randall, J. Guo, Z. M. Qi, T. Shao, X. Yao, *RSC Adv.* **2013**, *3*, 5009.
[39] S. Wang, P. Chen, J. H. Yun, Y. Hu, L. Wang, *Angew. Chem., Int. Ed.* **2017**, *56*, 8500.
[40] X. Xu, Y. Xu, F. Xu, G. Jiang, J. Jian, H. Yu, E. Zhang, D. Shchukin, S. Kaskel, H. Wang, *J. Mater. Chem. A* **2020**, *8*, 1636.
[41] G. Wang, Y. Ling, X. Lu, F. Qian, Y. Tong, J. Z. Zhang, V. Lordi, C. Rocha Leao, Y. Li, *J. Phys. Chem. C* **2013**, *117*, 10957.
[42] X. Zhang, X. Du, *New J. Chem.* **2020**, *44*, 1703.
[43] R. A. Eichel, *Phys. Chem. Chem. Phys.* **2010**, *13*, 368.
[44] J. D. Prades, J. Arbiol, A. Cirera, J. R. Morante, M. Avella, L. Zanotti, E. Comini, G. Faglia, G. Sberveglieri, *Sens. Actuators B, Chem.* **2007**, *126*, 6.
[45] L. Francàs, S. Corby, S. Selim, D. Lee, C. A. Mesa, R. Godin, E. Pastor, I. E. L. Stephens, K. S. Choi, J. R. Durrant, *Nat. Commun.* **2019**, *10*, 1.
[46] D. K. Lee, K. S. Choi, *Nat. Energy* **2017**, *3*, 53.
[47] B. Klahr, S. Gimenez, F. Fabregat-Santiago, T. Hamann, J. Bisquert, *J. Am. Chem. Soc* **2012**, *134*, 36.
[48] R. Yalavarthi, R. Zbořil, P. Schmuki, A. Naldoni, Š. Kment, *J. Power Sources* **2021**, *483*, 229080.
[49] Q. Shi, S. Murcia-López, P. Tang, C. Flox, J. R. Morante, Z. Bian, H. Wang, T. Andreu, *ACS Catal.* **2018**, *8*, 3331.
[50] Y. Hermans, S. Murcia-López, A. Klein, W. Jaegermann, *ACS Energy Lett.* **2019**, *4*, 2522.
[51] F. M. Toma, J. K. Cooper, V. Kunzelmann, M. T. McDowell, J. Yu, D. M. Larson, N. J. Borys, C. Abelyan, J. W. Beeman, K. M. Yu, J. Yang, L. Chen, M. R. Shaner, J. Spurgeon, F. A. Houle, K. A. Persson, I. D. Sharp, *Nat. Commun.* **2016**, *7*, 1.